ČESKÉ VYSOKÉ UČENÍ TECHNICKÉ
Stavební fakulta
Katedra mechaniky

Modular-Topology Optimization of Truss Structures Composed of Wang Tiles

Modularní topologická optimalizace příhradových konstrukcí složených z Wangových dlaždic

Rektorysova soutěž

Studijní program:	Stavební inženýrství
Studijní obor:	Konstrukce pozemních staveb
Vedoucí práce:	Doc. Ing. Jan Zeman, Ph.D.

Bc. Marek Tyburec

Praha 2016

Contents

1 Introduction **2**

2 Background **3**
2.1 Vertex-Based Tiling 3
2.2 Truss Optimal Design 3

3 Methodology **6**
3.1 Topology Optimization of Modular Truss Structures 6
3.2 Assembly Plan Optimization 8

4 Examples **9**
4.1 Coarsely Discretized Beam 9
4.1.1 Relation Between Connectivity Matrix and Design Quality 11
4.2 Finely Discretized Beam 12

5 Conclusions **14**

1 Introduction

Finding optimal structures has been a challenging task in the interest of many researchers, see e.g. [5] for an overview. The so-called structural optimization usually tries to achieve one (or more) of the following objectives: the structure of minimum weight, the most stiff structure or the structure as insensitive to instability and buckling as possible.

Although several different objectives exist, they have something in common – they approximately denote the requirement of an investor to be economical. For mass production, however, another aspect is also important – modularity. Prefabricated modular products are produced off-site in controlled environments, leading to high-quality products and significant time savings by a parallel execution of several building phases.

Optimal distribution of material within structure can be viewed from two scales: the macro-scale and the micro-scale levels. Due to enormous computational demands when dealing with both the levels concurrently, these two scales are commonly being separated, see eg. [24], resulting in microstructures being tailored at specific property [6], rather than at specific application [2]. Another drawback of the multi-scale model is the lack of the ability to constrain adjacent microstructural cells to be compatible on edges [2], limiting thus possible industrial utilization.

To deal with the problem of connectivity of cells, several approaches have been developed. While some rely on post-processing of cells by smoothening material distribution across their edges [19], another utilize periodic or layered microstructures [2]. In [21] a single microstructural cell is gradated along specified dimensions, leading to stretching and extensions of the cell. However, all the present approaches involve microstructural periodicity.

In this paper we approximate the microstructural cells with trusses, similarly to [1], and utilize aperiodic vertex-based Wang tiling [15] to describe their assembly plan. Finally, we optimize concurrently the assembly plan of individual tiles (modules) and their topology through two-level optimization approach, consisting of second-order cone programming and genetic algorithm. The developed approach is applied on an example beam.

2 Background

2.1 Vertex-Based Tiling

The idea of domino-like Wang tiles has been firstly proposed in [23] by Hao Wang, hence the name Wang tiles. Wang tiles are a set of squares with colored edges and fixed orientation. To create valid tiling the tiles are placed next to each other in a way that the adjoining edges are assigned the same color.

Because continuity of the tiling enforced by colored edges and ability of some tile sets to efficiently tile aperiodic patterns [10], Wang tiles are used in computer graphics for texture synthesis, tile-based texture mapping and for generation of Poisson disk distributions [7]. The colored edges can not, however, secure non-violation of continuity by formation of artifacts in the close surroundings to tile corners. To solve the so-called corner problem [7], corner tiles, with the connectivity information stored in colored corners, have been developed [15]. Their other advantages compared to the classical edge-based Wang tiles lie in simpler generation of valid tiling, reduced memory requirements and simpler generalization to multiple dimensions.

In this paper we adopt the corner tiles, but call them *vertex-based* Wang tiles to highlight their simple generalization to 3D and simultaneously preserve terminology among dimensions. The complete set of the planar vertex-based tiles over two colors, used throughout this paper, contains one vertex-based tile for each possible combination of colors, as shown in Fig 1.

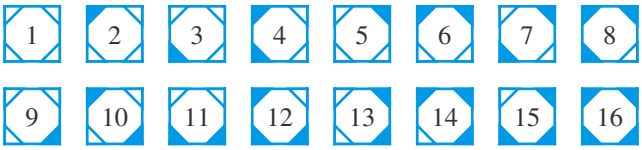

Figure 1: The complete set of vertex-based Wang tiles over two colors.

To create a valid assembly plan of the tiling the vertex-based tiles are placed such that the vertex shared by surrounding tiles has the same color; compare Fig. 2b and 2c. Each color is assigned an integer value [15], here we use 0 for white and 1 for blue, so that rectangular tiling can be described by connectivity matrix $\mathbf{C} \in \{0,1\}^{(n_{\mathrm{t,y}}+1)\times(n_{\mathrm{t,x}}+1)}$, with $n_{\mathrm{t,y}} \in \mathbb{Z}_{>0}$ and $n_{\mathrm{t,x}} \in \mathbb{Z}_{>0}$ being the numbers of tiles in vertical and horizontal direction, respectively. The unique equivalence between the connectivity matrix and the assembly plan is shown in Fig. 2a and 2b.

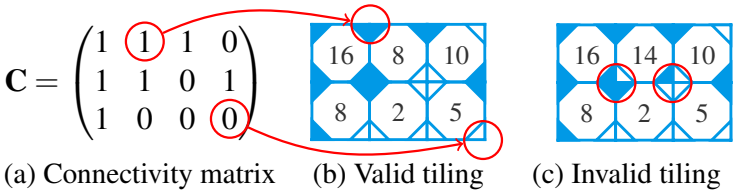

(a) Connectivity matrix (b) Valid tiling (c) Invalid tiling

Figure 2: Illustration of: (a) connectivity matrix and its correspondence to valid tiling (b), (c) example of invalid tiling.

Utilizing the complete set of vertex-based tiles over a limited set of colors secures that all tilings, described by any connectivity matrix containing only the integer values assigned to the color set, are valid.

2.2 Truss Optimal Design

Trusses are structures consisting of joints and straight bars transmitting only axial forces. Optimal topology of the least compliant truss, for a given boundary conditions, should have the most of its structural stiffness aligned with the principal strains [17], whose trajectories are generally not straight.

Subsequently, the optimal design may contain infinite number of bars, making the fabrication impossible. Therefore, the fixed design domain $\mathscr{D}$ is usually discretized into a finite design space consisting of a set of n_j fixed admissible joints and n_b feasible bars. The discretization is usually referred to as ground-structure [9].

Common design variables of the optimization are cross-sectional areas $\mathbf{a} \in \mathbb{R}^{n_\mathrm{b}}_{\geq 0}$, having the possibility to attain zero values. Through the convergence process the bars that do not contribute to structural stiffness are removed and topology of the truss is altered. Therefore, this type of optimization is called *topology* optimization [5].

In truss topology optimization there exist several approaches towards finding the optimal design. In traditional *plastic design* [9] the problem is stated in member forces only, trying to obtain the best topology under static equilibrium constraint and bounds on allowed stresses; neglecting kinematic compatibility. The optimization converges to a statically determinate[1] solution [22] automatically fulfilling the compatibility conditions [5], but only, when a single load case is considered. Similarly to the multiple loads [18], enforcing modularity into the plastic formulation generally leads to statically indeterminate optimal designs, implying that the static equilibrium is not uniquely solvable and without kinematic compatibility the axial forces are not distributed based on stiffnesses. Subsequently, the strains generate stresses that are not, in general, within the prescribed bounds. Hence, plastic formulation is not appropriate for modular design and kinematic compatibility needs to be considered.

The plastic design does, however, create a lower-bound [5] to the well-known *elastic design* formulation. In this paper we aim at finding the least-compliant design subjected to a volume constraint (1c) and compatibility conditions (1b). The optimization problem is then stated as

$$\begin{aligned}
\min_{\mathbf{a}\in\mathbb{R}^{n_\mathrm{b}},\mathbf{u}\in\mathbb{R}^{n_\mathrm{dof}}} \quad & \frac{1}{2}\mathbf{f}^\mathrm{T}\mathbf{u} && \text{(1a)}\\
\text{s.t.} \quad & \mathbf{K}(\mathbf{a})\mathbf{u} = \mathbf{f}, && \text{(1b)}\\
& \mathbf{l}^\mathrm{T}\mathbf{a} \leq \overline{V}, && \text{(1c)}\\
& \mathbf{a} \geq \mathbf{0}, && \text{(1d)}
\end{aligned}$$

where $\mathbf{f} \in \mathbb{R}^{n_\mathrm{dof}}$ denotes nodal forces column vector, $n_\mathrm{dof} \in \mathbb{Z}_{>0}$ refers to the number of degrees of freedom, $\mathbf{u} \in \mathbb{R}^{n_\mathrm{dof}}$ stands for displacements column vector, $\mathbf{K(a)} \in \mathbb{R}^{n_\mathrm{dof}\times n_\mathrm{dof}}$ is structural stiffness matrix, $\mathbf{l} \in \mathbb{R}^{n_\mathrm{b}}$ stands for a column vector of bars' lengths and $\overline{V} \in \mathbb{R}_{>0}$ denotes an upper-bound on total structural volume. The objective of the optimization $c = \frac{1}{2}\mathbf{f}^\mathrm{T}\mathbf{u}$, $c \in \mathbb{R}_{>0}$ (1a) is compliance, the work done by nodal forces. The lower the compliance, the stiffer is the truss with respect to prescribed loads.

The formulation (1) is a nonlinear non-convex optimization problem, which is therefore hard to solve [14]. Based on [16] and Section 3.4.3 in [4] it can be, however, reformulated as a convex second-order cone program (SOCP)

$$\begin{aligned}
\min_{\mathbf{a}\in\mathbb{R}^{n_\mathrm{b}},\boldsymbol{\tau}\in\mathbb{R}^{n_\mathrm{b}},\mathbf{s}\in\mathbb{R}^{n_\mathrm{b}}} \quad & \frac{1}{2}\sum_{i=1}^{n_\mathrm{b}} \tau_i && \text{(2a)}\\
\text{s.t.} \quad & \mathbf{l}^\mathrm{T}\mathbf{a} \leq \overline{V}, && \text{(2b)}\\
& \sum_{i=1}^{n_\mathrm{b}} s_i\sqrt{\frac{E}{l_i}}\mathbf{r}_i = \mathbf{f}, && \text{(2c)}\\
& \left\| \begin{pmatrix} \sqrt{2}s_i \\ \frac{2a_i-\tau_i}{2} \end{pmatrix} \right\|_2 \leq \frac{2a_i+\tau_i}{2}, \quad \forall i \in \{1\,..\,n_\mathrm{b}\} && \text{(2d)}\\
& \mathbf{a} \geq 0, && \text{(2e)}
\end{aligned}$$

[1] Statically determinate design means that the axial forces can be uniquely determined from the static equilibrium only [18].

that is efficiently solvable to global optimality by interior-point methods [3] by several available solvers. In Eq. (2) the symbol $s_i \in \mathbb{R}$ stands for axial force of the i-th bar, $E \in \mathbb{R}_{>0}$ denotes modulus of elasticity, l_i is the length of i-th bar and $\mathbf{r}_i \in \mathbb{R}^{n_{\mathrm{dof}}}$ denotes the i-th column of the static matrix $\mathbf{A} \in \mathbb{R}^{n_{\mathrm{dof}} \times n_{\mathrm{b}}}$. The objective (2a) is equal to compliance.

It should be also noted that the notation $\|\cdot\|_2$ denotes L_2 norm, so that $\|\mathbf{x}\|_2$, $\mathbf{x} \in \mathbb{R}^2$ describes a second-order cone.

3 Methodology

Let us assume fixed design domain $\mathscr{D}$ defining structural dimensions, and boundary conditions. In order to achieve modularity of the structure the design domain is discretized into a rectangular grid, forming tiles, see Fig. 3.

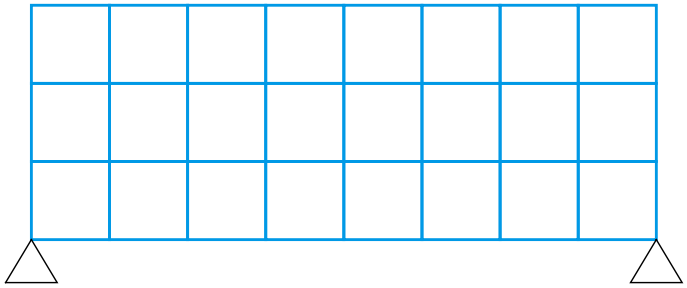

Figure 3: Example of a discretized design domain.

The discretized design domain is tiled by a limited set of n_t repeating tiles (modules), where n_t should be sufficiently low to sustain modularity. Also, the neighboring tiles need to be compatible to produce statically admissible structure that is able to transmit external loading to the supports. To constrain feasible neighbors of each tile type in the set of n_t tiles, vertex-based Wang tiles [15] over two colors are used, so that $n_\mathrm{t} = 16$ contains the complete tile set. Wang tiles then add the ability to define four unique types of horizontal and vertical edges, respectively, grant absolute compatibility between fitting tile edges and subsequently provide behavior likewise jigsaw puzzle, recall Fig. 2.

In this paper we utilize truss tiles building together ground structure. For the optimization it is proposed a two-level approach: in the upper level the assembly plan defining Wang tiling is optimized with respect to the lower level – modular topology optimization.

3.1 Topology Optimization of Modular Truss Structures

The lower-level optimization aims at minimization of compliance for a given assembly plan with a constraint on volume and elastic equilibrium, recall the optimization problem formulation (2).

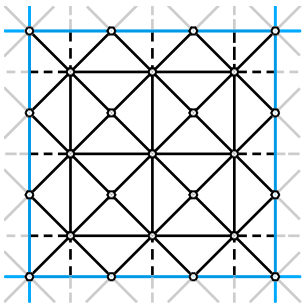

Figure 4: Ground structure of a tile. The black solid lines represent tile-associated bars, the dashed lines denote edge-associated bars. Scattered points represent joints.

All truss tiles from the tile set are defined to have the same tile ground structure, see Fig. 4 for reference. Bars in all tiles are divided into three sets: ones lying *only* in the interior of a tile, called *tile-associated*, are bound solely to the specific tile type in which they lie, such bars are drawn in Fig. 4 by solid black lines; bars coming through any edge of the tile, so that they do not start or end on the edge, are called *edge-associated*, because they are tied to the edge type; in Fig 4 they are drawn by dashed line. Similarly, it is further possible to introduce *vertex-associated* bars that come through a vertex of a tile and do not start or end there. These bars would then be bound to the specific vertex type, they are not, however, used in this paper; we list them just for the sake of completeness.

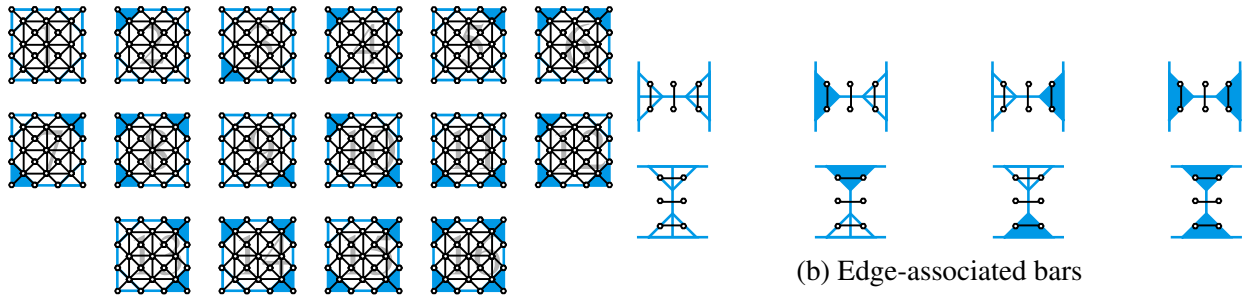

(a) Tile-associated bars

(b) Edge-associated bars

Figure 5: Division of bars into tile-associated (a) and edge-associated (b). The scattered point represent joints.

Afterwards, it is needed to ensure the same topology across equal tile types and equal edge types. This has been done through division of bars into groups, such that all bars in the same group are assigned the same cross-sectional area. Assignment of groups to bars is provided by so-called group vector $\mathbf{g}(\mathbf{C}) \in \mathbb{Z}_{>0}^{n_\mathrm{b}}$. The group vector assigns each bar of the ground structure a single number in the range of $\{1 \,..\, n_\mathrm{g}\}$, with n_g denoting the number of groups. If we evaluate, for example, the complete tile set built by tiles depicted in Fig. 4, we obtain $16 \times 48 = 768$ groups of tile-associated bars, as the complete tile set contains 16 tiles and each tile consists of 48 tile-associated bars, see Fig. 5a; similarly, each edge of the tile includes 3 edge-associated bars, so that 4 vertical and 4 horizontal types of edges yields totally $2 \times 4 \times 3 = 24$ groups of edge-associated bars, see Fig. 5b. We have therefore $n_\mathrm{g} = 792$ altogether.

From the group vector it is further possible to asses group matrix $\mathbf{G}(\mathbf{C}) \in \{0,1\}^{n_\mathrm{b} \times n_\mathrm{g}}$ that is defined $\forall i \in \{1 \,..\, n_\mathrm{b}\}$ and $\forall j \in \{1 \,..\, n_\mathrm{g}\}$ as

$$\mathbf{G}(i,j) = \begin{cases} 0 & \text{for } j \neq \mathbf{g}(i) \\ 1 & \text{for } j = \mathbf{g}(i) \end{cases}. \tag{3}$$

By introduction of groups the original topology optimization formulation (2) is modified, reducing the count of cross-sectional areas from n_b to n_g, as they are substituted by grouped cross-sectional areas $\mathbf{a}_\mathrm{g} \in \mathbb{R}_{\geq 0}^{n_\mathrm{g}}$. Consequently, the volume constraint (2b) transforms into

$$\mathbf{l}^\mathrm{T} \mathbf{G}(\mathbf{C}) \mathbf{a}_\mathrm{g} \leq \overline{V} \tag{4}$$

and the second-order cone constraint (2d) translates into

$$\left\| \begin{pmatrix} \sqrt{2} s_i \\ \frac{2a_{g,g_i} - \tau_i}{2} \end{pmatrix} \right\|_2 \leq \frac{2a_{g,g_i} + \tau_i}{2}, \quad \forall i \in \{1 \,..\, n_\mathrm{b}\}, \tag{5}$$

with a_{g,g_i} being the grouped cross-sectional area belonging to the i-th element of the group vector $\mathbf{g}(\mathbf{C})$.

The final formulation of modular topology optimization is then

$$\min_{\mathbf{a_g}\in\mathbb{R}^{n_\mathrm{g}},\boldsymbol{\tau}\in\mathbb{R}^{n_\mathrm{b}},\mathbf{s}\in\mathbb{R}^{n_\mathrm{b}}} \quad \frac{1}{2}\sum_{i=1}^{n_\mathrm{b}}\tau_i \tag{6a}$$

$$\text{s.t.} \quad \mathbf{l}^\mathrm{T}\mathbf{G}(\mathbf{C})\mathbf{a}_\mathrm{g} \leq \overline{V}, \tag{6b}$$

$$\sum_{i=1}^{n_\mathrm{b}} s_i\sqrt{\frac{E}{l_i}}\mathbf{r}_i = \mathbf{f}, \tag{6c}$$

$$\left\|\begin{pmatrix}\sqrt{2}s_i \\ \frac{2a_{g,g_i}-\tau_i}{2}\end{pmatrix}\right\|_2 \leq \frac{2a_{g,g_i}+\tau_i}{2}, \quad \forall i\in\{1\,..\,n_\mathrm{b}\} \tag{6d}$$

$$\mathbf{a_g} \geq 0. \tag{6e}$$

3.2 Assembly Plan Optimization

Let us define an operator $M\colon \mathbf{C}\mapsto c$ that maps, through the convex modular topology formulation (6), the space of binary connectivity matrices $\mathbf{C}\in\{0,1\}^{(n_{\mathrm{t,y}}+1)\times(n_{\mathrm{t,x}}+1)}$ into scalar space $c\in\mathbb{R}_{>0}$. Then, the upper-level optimization searches such an assembly plan $\mathbf{C}^*$, for which it stands that

$$c^* = M(\mathbf{C}^*) \tag{7}$$

and

$$c^* = \min\{c\in\mathbb{R}_{>0}, c = M(\mathbf{C}), \mathbf{C}\in\{0,1\}^{(n_{\mathrm{t,y}}+1)\times(n_{\mathrm{t,x}}+1)}\}, \tag{8}$$

which is a (non-convex) NP-complete combinatorial problem with globally optimal connectivity matrix $\mathbf{C}^*$ and globally optimal compliance c^*. To emphasize the influence of the connectivity matrix $\mathbf{C}$ on the objective value the reader is referred to the Section 4, especially to Fig. 7b and Fig. 8a.

Due to the nature of (8) its direct solution is difficult even for small-scale problems, as there does not exist any deterministic polynomial time algorithm for its solution, in the meaning of $\mathbf{C}^*$ and c^*. Therefore, we have adopted meta-heuristic genetic algorithm (GA) [12] that has proved convergence to solutions near global optimum.

GA is a stochastic optimization algorithm that mimics natural process of evolution. Through generations the initial population evolves. Following the natural selection, individuals with higher fitnesses (i.e. lower c in our case) are preferred to give birth to offspring, who inherit the most of their parents' genetic information through so-called cross-over, improving the overall population fitness. As in real life, offspring's genes might also become mutated, which contributes to diversity of individuals.

In the optimization of assembly plan the genetic information, chromosome, is represented by connectivity matrix $\mathbf{C}$, as it uniquely determines the fitnesses of individuals. Therefore, the initial random population is generated by random connectivity matrices.

Offspring are born by cross-over of two parents chosen by tournament selection. The offspring inherit its genetic information from both its parents through uniform cross-over with probability of 0.94. The genes are mutated with probability of $1/n_{\mathrm{el,C}}$, with $n_{\mathrm{el,C}}$ denoting the number of elements of $\mathbf{C}$. Afterwards, the old generation dies except for an elite individual with highest fitness value, who joins just born population, to avoid losing the best solution. To extend the search space of algorithm, we have also enforced diversity of the population, replacing duplicate individuals by new ones randomly generated.

4 Examples

The proposed approach has been successfully implemented in MATLAB and applied on example design of a planar hinge-supported beam. Firstly, a relatively coarse discretization is utilized in order to provide comparison of results of the two-level optimization with global optimum obtained by brute-force enumeration. Subsequently, we also present fine discretization and compare the coarse and fine designs.

All the computations have been performed on Intel® Xeon® E5-2630 with 32 logical cores and 128 GB RAM. Modular topology optimization (6) have been solved by commercial solver Gurobi [11].

4.1 Coarsely Discretized Beam

The example beam of dimensions 8×3 m, see Fig. 6, is discretized into 24 tiles, each of the unit size, and tiled by a complete set of vertex-based Wang tiles, with all the tiles having the same tile ground structure, as shown in Fig. 4. The bars are prescribed Young's modulus E equal to 1 Pa. Boundary conditions are stated as follows: hinge supports are located in the very bottom-left and bottom-right corners of the beam; and an external force with magnitude of 10 N acts in the midspan of the beam, causing bending. It should be noted that the selected properties do not describe any specific material nor realistic situation and have been chosen only to avoid scaling of the optimization problem and concurrently provide numerical stability.

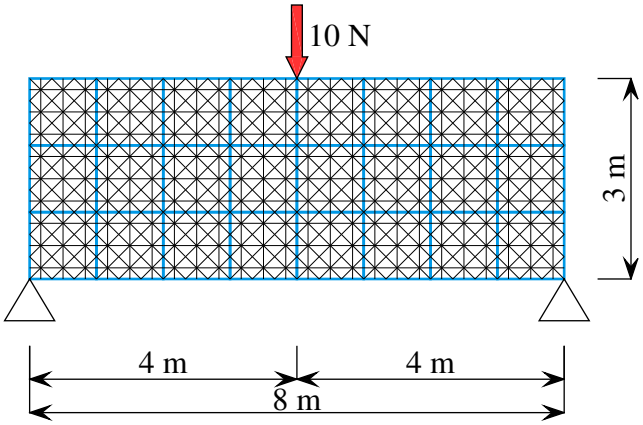

Figure 6: Dimensions, discretization, boundary conditions and ground structure of the example beam.

The price of modularity is clearly a worse compliance [13]. Because all tiles from the complete tile set are defined to have the same tile ground structure the ground structure can be uniquely assessed. Subsequently, it is possible to state an ideal objective value by performing topology optimization without application of groups (2), resulting in a lower-bound to c^* (8). Considering the evaluated example we obtain $c_{\text{ideal}} = 61.9$ Nm, as shown in Fig. 7a. Reached objective value, naturally, can not be overcome in any modular design, given the same ground structure, but it is advisable to get close to the attained lower-bound as much as possible.

Similarly to the ideal design it is straightforward to obtain an upper-bound worst-case objective value by tiling the beam by only one tile type, i.e. the connectivity matrix $\mathbf{C}$ containing all zeros or all ones. The result of the worst-case topology optimization with optimal objective $c_{\text{worst}} = 191.2$ Nm is shown in Fig. 7b. Based on the ideal and worst-case objective bounds it implies that $c^* \in [61.9, 191.2]$ Nm.

In order to compare designs reached by two-level optimization, proposed in Section 3, with proven globally optimal solution obtained by brute-force enumeration, we have enforced symmetricity of the connectivity matrix $\mathbf{C}$ along midspan of the beam, limiting thus the number of combinations of assembly plans from 2^{40} to 2^{20}. Although such assumption dramatically decreases the problem

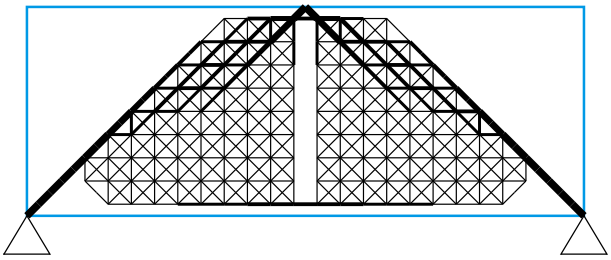

(a) Ideal design, $c_{\text{ideal}} = 61.9$ Nm

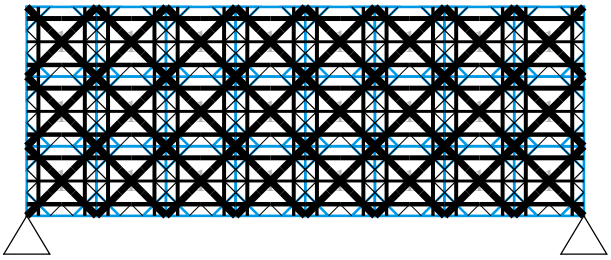

(b) Worst-case design, $c_{\text{worst}} = 191.2$ Nm

Figure 7: Lower-bound (a) and upper-bound (b) solutions to c^*.

size, it should be noted that the global optimum might not be identical to the case without enforced symmetricity.

The number of combinations can be further reduced by recognizing the fact that the vertex types do not have any actual physical meaning; therefore topology optimization of any assembly plan denoted by $\mathbf{C}$ yields equal result to the optimization of reversed $\mathbf{C}$ (that is $\mathbf{C}$ having interchanged all 0 with 1 and vice-versa). Subsequently, it is needed to enumerate 2^{19} combinations.

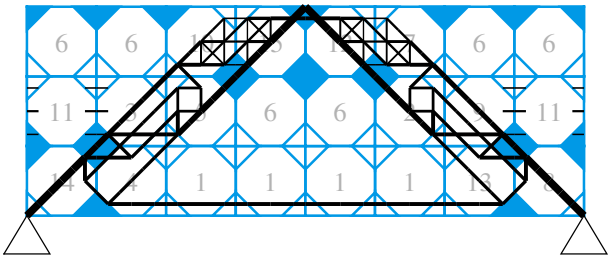

(a) Globally optimal design

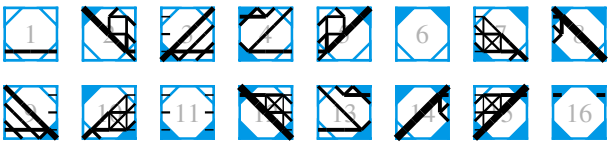

(b) Globally optimal tile set

Figure 8: Globally optimal design (a) and tile set (b) of the coarsely discretized beam with $c^* = 62.7$ Nm.

Evaluation of all the combinations took 9.5 hours. Throughout the enumeration globally optimal design with $c^* = 62.7$ Nm has been obtained, see Fig. 8a, being thus only 1.3 % more-compliant than the ideal design. The tile set of the globally optimal design, shown in Fig. 8b, contains 13 non-empty tiles, making 3 empty tiles to be potentially omitted. Overall, the enumerated combinations generate nearly Gaussian distribution with the mean value of 107.7 Nm and standard deviation equal to 14.6 Nm, see Fig. 9.

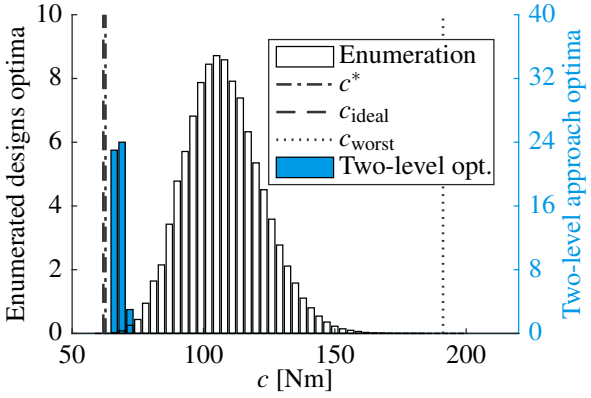

Figure 9: Comparison of the results achieved by brute-force enumeration and the proposed two-level optimization.

The actual two-level optimization was launched 50 times, each time with different random population of 16 individuals, evaluating the statistical properties of the two-level optimization approach. The convergence of c of the best individuals and the mean value of all runs though generations are shown in the Fig. 10.

The initial random populations uniquely determine topologies of mean objective value equal to 107.4 Nm, being thus in a fair correspondence with the mean value 107.7 Nm of the nearly Gaussian distribution. Throughout prescribed 40 generations of the genetic algorithm the objective decrease to the final mean value of the best individual 67.4 Nm, being in average 8.9 % worse than the ideal solution and 7.5 % worse than the global optimum. Through the two-level optimization the second best solution has been reached. Totally, all the achieved objectives are within the lowest 0.2 % of all the combinations, recall Fig. 9.

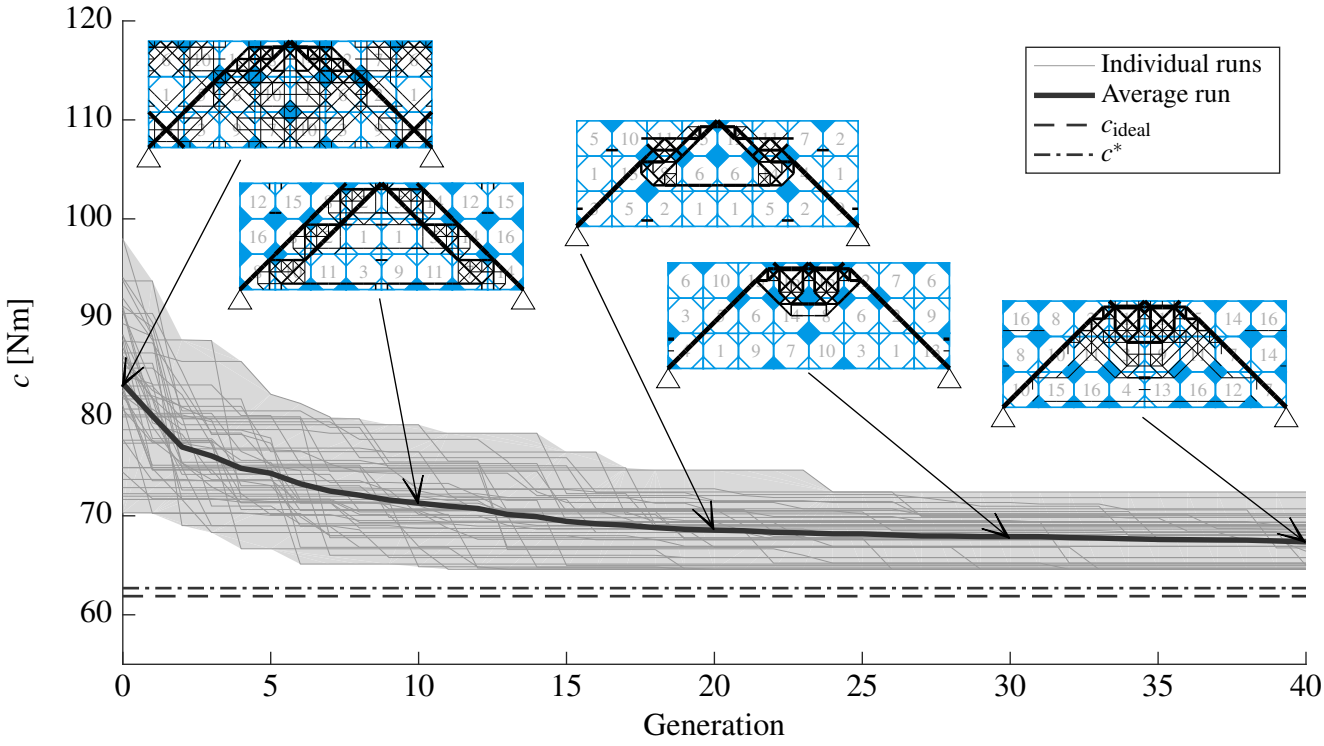

Figure 10: Convergence of 50 independent runs of the proposed two-level optimization approach with random population. Displayed designs sample the convergence of the algorithm.

4.1.1 Relation Between Connectivity Matrix and Design Quality

Another question of interest is existence of a relation between quality of designs with respect to connectivity matrices, to permit creation of quality designs from scratch.

The first evaluated aspect is a ratio of zero and nonzero elements in the connectivity matrix. By plotting all the enumerated combinations it is obtained a boxplot shown in Fig. 11, from which it implies that better designs, with the lowest mean objective value and smallest variance, are obtained when the number of nonzero elements in $\mathbf{C}$ is equal to the number of zeros in $\mathbf{C}$. However, enforcing such assumption into optimization might also avoid the global optimum, as in this example.

Secondly, it obvious from the worst-case design that the quality depends on the number of tiles that are utilized from the complete tile set. All the enumerated combinations create a boxplot shown in Fig. 12, leading to the conclusion that the higher the number of utilized tiles, the better design should we, averagely, expect. Again, strictly enforcing such assumption might avoid the global optimum.

Finally, to provide a good guess of the connectivity matrix that determines a low-compliant design, the matrix should consist of similar counts of nonzero and zero elements and the resulting assembly

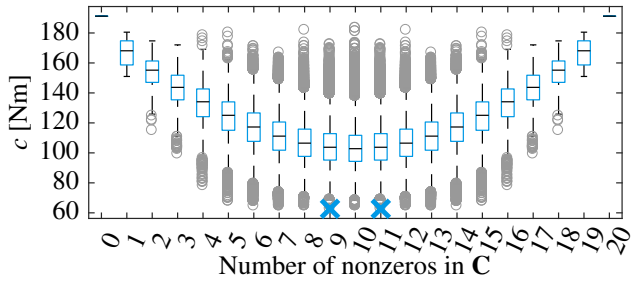

Figure 11: Compliance as a functional of the count of nonzero elements in symmetric part of $\mathbf{C}$ of the example beam. The crosses denote global optimum.

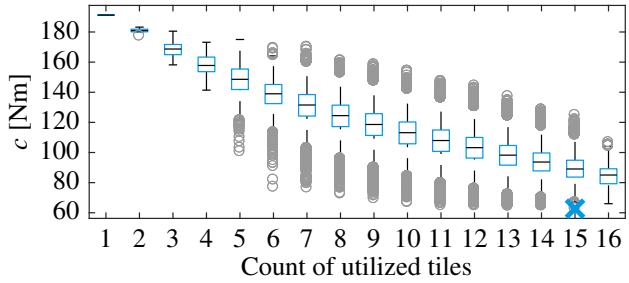

Figure 12: Compliance as a functional of the count of utilized tiles in the example beam with enforced symmetricity of $\mathbf{C}$. The cross denotes global optima.

plan should contain, if possible, all the tiles from the complete tile set.

4.2 Finely Discretized Beam

Let us consider the same design domain, recall Fig. 6, finely tiled by 16×6 tiles of a side length equal to 0.5 m. To sustain comparability with the previous case, it is again enforced symmetricity of the connectivity matrix, allowing thus 2^{62} unique combinations of optimal topologies.

Such a huge amount of combinations and larger number of degrees of freedom make it impossible to perform brute-force enumeration that have been accomplished in the coarse discretization; so that we are left in the proposed two-level optimization without the knowledge of the true global optimum. It is, however, similarly to the previous example, straightforward to obtain the ideal compliance $c_{\text{ideal}} = 61.1$ Nm, refer to Fig. 13a, and the worst-case compliance $c_{\text{worst}} = 228.7$ Nm, see Fig. 13b, so that $c^* \in [61.1; 228.7]$ Nm.

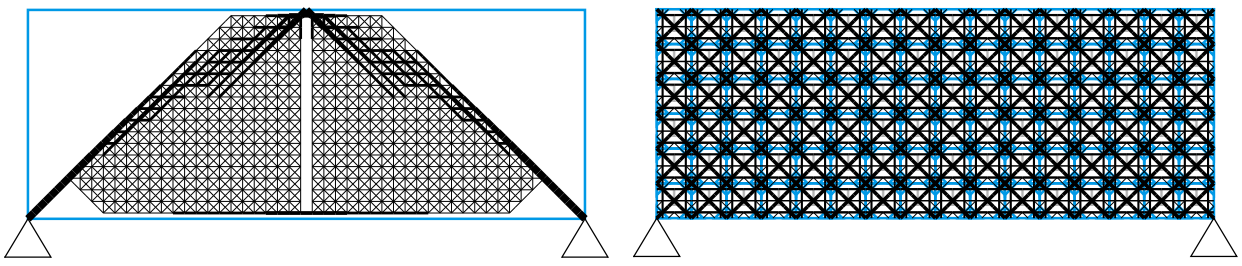

(a) Ideal design, $c_{\text{ideal}} = 61.1$ Nm

(b) Worst-case design, $c_{\text{worst}} = 228.7$ Nm

Figure 13: Lower-bound (a) and upper-bound (b) solutions to c^*.

Compared to the coarse discretization, fine discretization produces richer ground structure, decreasing thus slightly the ideal objective value. On the contrary, the worst-case objective noticeably increases, as more tiles are constrained to satisfy all boundary conditions, i.e. transmit the force. Such a consequence of modularity has also been reported in [13].

The two-level optimization was launched 20 times, see Fig. 14 for convergence of the algorithm. The initial random populations of 29 individuals determine designs of mean objective value 156.5 Nm, significantly increased (45.3 %) compared to the coarse discretization. Throughout 70 generations the two-level optimization converged to the mean objective value of 82.1 Nm, being 34.4 % more-compliant than the ideal design. The best reached design with $c = 71.6$ Nm is shown in Fig. 15, being 17.0 % worse than the ideal compliance.

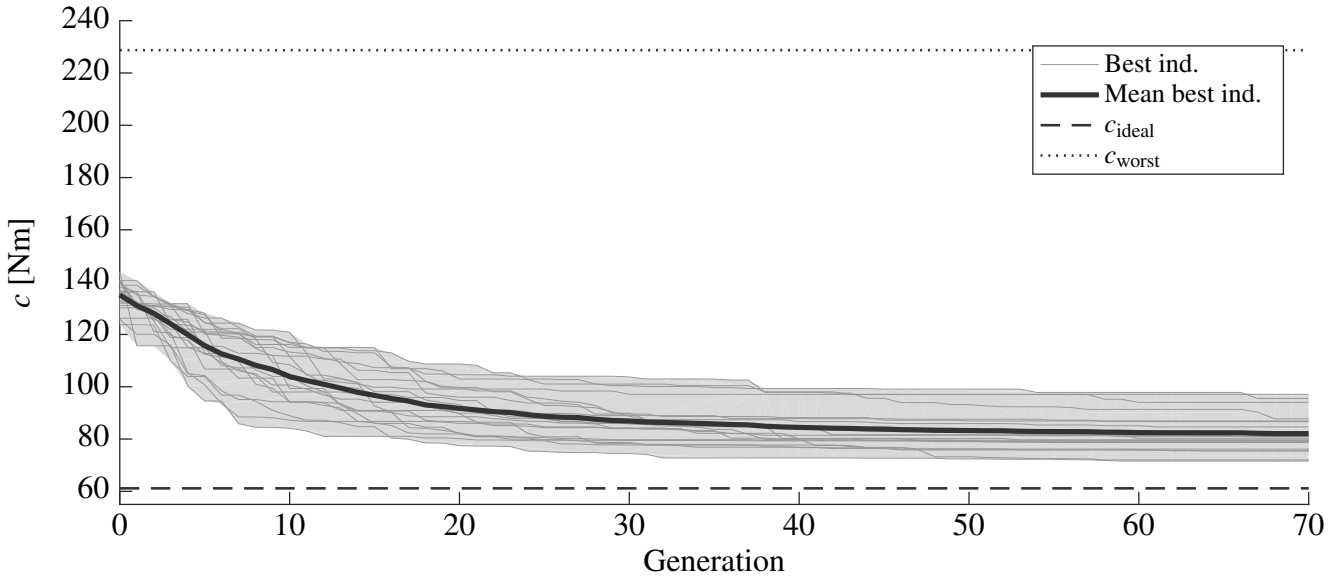

Figure 14: Convergence of 20 independent runs of the proposed two-level optimization approach with random initial population applied on finely discretized example beam.

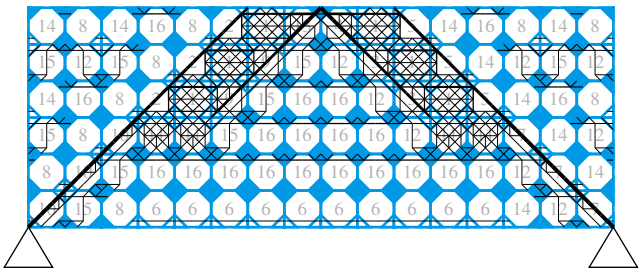

Figure 15: Best design ($c = 71.6$ Nm) of finely discretized example beam obtained through the two-level optimization.

5 Conclusions

Throughout this paper a novel two-level optimization approach producing modular trusses has been developed. The lower-level optimization represents standard truss topology least-compliant design problem extended to structural modularity using groups. The optimization problem is formulated as a convex SOCP that is efficiently solvable to global optimality.

Structural modularity is explicitly stated by an assembly plan of vertex-based Wang tiles over two colors, generating thus 16 unique modules and securing compatibility and continuity among edges. Because for any assembly plan there exists a unique globally optimal solution to the lower-level modular topology optimization, the upper-level optimization aims at finding such an assembly plan, for which it is obtained the least-compliant topology overall. Because the upper-level optimization makes the problem non-convex combinatorial, we propose to solve it by meta-heuristic genetic algorithm.

The developed approach has been successfully demonstrated on a solution of example beam, proving, that enforcing modularity to the structure might increase compliance only marginally (1.3 %) compared to the ideal non-modular beam, while utilizing 13 nonempty tiles. The two-level optimization secures convergence to solutions near global optimum, so that in the example all achieved designs lie below the 0.2 % quantile of all designs.

In the near future it is planned to extend the approach to 3D, so that the optimal tile sets could be applied in modular design of 3D-printed lego-like products [20] or combinatorial aperiodic metamaterials [8]. It is also of interest to extend the formulation to continuum framework [2].

Acknowledgements

The author would like to express sincere gratitude to Doc. Ing. Jan Zeman, Ph.D., Ing. Martin Doškář, Doc. Ing. Matěj Lepš, Ph.D. and Prof. RNDr. Michal Kočvara, DrSc. for inspiring comments and fruitful ideas.

The author acknowledges the financial support from the Grant Agency of the CTU in Prague, through project No. SGS16/037/OHK1/1T/11, and from the Czech Science Foundation, through project No. 14-00420S.

References

[1] *Some Inverse Problems in Topology Design of Materials and Mechanisms*. URL: http://www.springerlink.com/index/10.1007/978-94-009-0153-7_35, doi:10.1007/978-94-009-0153-7_35.

[2] J. ALEXANDERSEN AND B. S. LAZAROV, *Topology optimisation of manufacturable microstructural details without length scale separation using a spectral coarse basis preconditioner*, Computer Methods in Applied Mechanics and Engineering, 290 (2015), pp. 156–182. doi:10.1016/j.cma.2015.02.028.

[3] M. F. ANJOS AND J. B. LASSERRE, eds., *Handbook on Semidefinite, Conic and Polynomial Optimization*, vol. 166 of International Series in Operations Research & Management Science, Springer US, Boston, MA, 2012. URL: http://link.springer.com/10.1007/978-1-4614-0769-0, doi:10.1007/978-1-4614-0769-0.

[4] A. BEN-TAL AND A. NEMIROVSKI, *Lectures on Modern Convex Optimization*, Society for Industrial and Applied Mathematics, Jan 2001. URL: http://citeseerx.ist.psu.edu/viewdoc/summary?doi=10.1.1.134.932, doi:10.1.1.134.932.

[5] M. P. BENDSØE AND O. SIGMUND, *Topology optimization: Theory, methods and applications*, Springer-Verlag, Berlin, Heidelberg, second ed., 2003. doi:10.1007/978-3-662-05086-6.

[6] M. P. BENDSØE AND N. KIKUCHI, *Generating optimal topologies in structural design using a homogenization method*, Computer Methods in Applied Mechanics and Engineering, 71 (1988), p. 197–224. doi:10.1016/0045-7825(88)90086-2.

[7] M. F. COHEN, J. SHADE, S. HILLER, AND O. DEUSSEN, *Wang tiles for image and texture generation*, ACM Transactions on Graphics, 22 (2003), pp. 287–294. URL: http://doi.acm.org/10.1145/882262.882265, doi:10.1145/882262.882265.

[8] C. COULAIS, E. TEOMY, K. DE REUS, Y. SHOKEF, AND M. VAN HECKE, *Combinatorial design of textured mechanical metamaterials*, Nature, 535 (2016), pp. 529–532. doi:10.1038/nature18960.

[9] W. S. DORN, R. E. GOMORY, AND H. J. GREENBERG, *Automatic design of optimal structures*, Journal de Mecanique, 3 (1964), pp. 25–52.

[10] B. GRÜNBAUM AND G. C. SHEPHARD, *Tilings and Patterns*, W. H. Freeman & Co., New York, NY, USA, 1986.

[11] I. GUROBI OPTIMIZATION, *Gurobi optimizer reference manual*, 2016. URL: http://www.gurobi.com.

[12] J. H. HOLLAND, *Adaptation in Natural and Artificial Systems: An Introductory Analysis with Applications to Biology, Control and Artificial Intelligence*, MIT Press, Cambridge, MA, USA, 1992.

[13] X. HUANG AND Y. M. XIE, *Optimal design of periodic structures using evolutionary topology optimization*, Structural and Multidisciplinary Optimization, 36 (2008), pp. 597–606. URL: http://link.springer.com/10.1007/s00158-007-0196-1, doi:10.1007/s00158-007-0196-1.

[14] M. KOČVARA AND J. V. OUTRATA, *Effective reformulations of the truss topology design problem*, Optimization and Engineering, 7 (2006), pp. 201–219. URL: http://link.springer.com/10.1007/s11081-006-6839-z, doi:10.1007/s11081-006-6839-z.

[15] A. LAGAE AND P. DUTRÉ, *An alternative for Wang tiles: Colored edges versus colored corners*, ACM Transactions on Graphics, 25 (2006), pp. 1442–1459. doi:10.1145/1183287.1183296.

[16] M. S. LOBO, L. VANDENBERGHE, S. BOYD, AND H. LEBRET, *Applications of second-order cone programming*, Linear Algebra and its Applications, 284 (1998), p. 193–228. URL: http://www-isl.stanford.edu/people/, doi:10.1016/S0024-3795(98)10032-0.

[17] A. G. M. MICHELL, *LVIII. The limits of economy of material in frame-structures*, The London, Edinburgh, and Dublin Philosophical Magazine and Journal of Science, 8 (1904), pp. 589–597. URL: http://www.tandfonline.com/doi/pdf/10.1080/14786440409463229.

[18] G. I. N. ROZVANY, T. SOKÓŁ, AND V. POMEZANSKI, *Fundamentals of exact multi-load topology optimization – stress-based least-volume trusses (generalized Michell structures) – Part I: Plastic design*, Structural and Multidisciplinary Optimization, 50 (2014), pp. 1051–1078. URL: http://link.springer.com/10.1007/s00158-014-1118-7, doi:10.1007/s00158-014-1118-7.

[19] A. RADMAN, X. HUANG, AND Y. M. XIE, *Topology optimization of functionally graded cellular materials*, Journal of Materials Science, 48 (2012), pp. 1503–1510. doi:10.1007/s10853-012-6905-1.

[20] C. SCHUMACHER, B. BICKEL, J. RYS, S. MARSCHNER, C. DARAIO, AND M. GROSS, *Microstructures to control elasticity in 3D printing*, ACM Trans. Graph., 34 (2015), pp. 136:1–136:13. doi:10.1145/2766926.

[21] L. L. STROMBERG, A. BEGHINI, W. F. BAKER, AND G. H. PAULINO, *Application of layout and topology optimization using pattern gradation for the conceptual design of buildings*, Structural and Multidisciplinary Optimization, 43 (2010), pp. 165–180. doi:10.1007/s00158-010-0563-1.

[22] G. SVED, *The minimum weight of certain redundant structures*, Australian J. Appl. Sci., 5 (1954), pp. 1–9.

[23] H. WANG, *Proving theorems by pattern recognition—II*, Bell system technical journal, 40 (1961), pp. 1–41. URL: http://onlinelibrary.wiley.com/doi/10.1002/j.1538-7305.1961.tb03975.x/abstract.

[24] L. XIA AND P. BREITKOPF, *Recent advances on topology optimization of multiscale nonlinear structures*, Archives of Computational Methods in Engineering, (2016), pp. 1–23. doi:10.1007/s11831-016-9170-7.